Inorganic Chemistry

Article

pubs.acs.org/IC

Syntheses and Electronic Properties of Rhodium(III) Complexes Bearing a Redox-Active Ligand

Sarath Wanniarachchi, Brendan J. Liddle, Brandon Kizer, Jeewantha S. Hewage, Sergey V. Lindeman, and James R. Gardinier*

Department of Chemistry, Marquette University, Milwaukee, Wisconsin 53201-1881, United States

Supporting Information

ABSTRACT: A series of rhodium(III) complexes of the redox-active ligand, H(**L** = bis(4-methyl-2-(1*H*-pyrazol-1-yl)phenyl)amido), was prepared, and the electronic properties were studied. Thus, heating an ethanol solution of commercial $RhCl_3 \cdot 3H_2O$ with H(**L**) results in the precipitation of insoluble [H(**L**)]$RhCl_3$, **1**. The reaction of a methanol suspension of [H(**L**)]$RhCl_3$ with NEt_4OH causes ligand deprotonation and affords nearly quantitative yields of the soluble, deep-green, title compound (NEt_4)[(**L**)$RhCl_3$]$\cdot H_2O$, **2**$\cdot H_2O$. Complex **2**$\cdot H_2O$ reacts readily with excess pyridine, triethylphosphine, or pyrazine (pyz) to eliminate NEt_4Cl and give charge-neutral complexes *trans*-(**L**)$RhCl_2$(py), *trans*-**3**, *trans*-(**L**)$RhCl_2(PEt_3)$, *trans*-**4**, or *trans*-(**L**)$RhCl_2$(pyz), *trans*-**5**, where the incoming Lewis base is *trans*- to the amido nitrogen of the meridionally coordinating ligand. Heating solutions of complexes *trans*-**3** or *trans*-**4** above about 100 °C causes isomerization to the appropriate *cis*-**3** or *cis*-**4**. Isomerization of *trans*-**5** occurs at a much lower temperature due to pyrazine dissociation. *Cis*-**3** and *cis*-**5** could be reconverted to their respective *trans*- isomers in solution at 35 °C by visible light irradiation. Complexes [(**L**)$Rh(py)_2Cl](PF_6)$, **6**, [(**L**)$Rh(PPh_3)$(py)Cl](PF_6), **7**, [(**L**)$Rh(PEt_3)_2Cl](PF_6)$, **8**, and [(**L**)RhCl(bipy)](OTf = triflate), **9**, were prepared from **2**$\cdot H_2O$ by using thallium(I) salts as halide abstraction agents and excess Lewis base. It was not possible to prepare dicationic complexes with three unidentate pyridyl or triethylphosphine ligands; however, the reaction between **2**, thallium(I) triflate, and the tridentate 4′-(4-methylphenyl)-2,2′:6′,2″-terpyridine (ttpy) afforded a high yield of [(**L**)Rh(ttpy)]-$(OTf)_2$, **10**. The solid state structures of nine new complexes were obtained. The electrochemistry of the various derivatives in CH_2Cl_2 showed a ligand-based oxidation wave whose potential depended mainly on the charge of the complex, and to a lesser extent on the nature and the geometry of the other supporting ligands. Thus, the oxidation wave for **2** with an anionic complex was found at +0.27 V versus Ag/AgCl in CH_2Cl_2, while those waves for the charge-neutral complexes **3**−**5** were found between +0.38 to +0.59 V, where the *cis*- isomers were about 100 mV more stable toward oxidation than the *trans*- isomers. The oxidation waves for **6**−**9** with monocationic complexes occurred in the range +0.74 to 0.81 V while that for **10** with a dicationic complex occurred at +0.91 V. Chemical oxidation of *trans*-**3**, *cis*-**3**, and **8** afforded crystals of the singly oxidized complexes, [*trans*-(**L**)$RhCl_2$(py)]$(SbCl_6)$, *cis*-[(**L**)$RhCl_2$(py)]$(SbCl_4) \cdot 2CH_2Cl_2$, and [(**L**)$Rh(PEt_3)_2Cl](SbCl_6)_2$, respectively. Comparisons of structural and spectroscopic features combined with the results of density functional theory (DFT) calculations between nonoxidized and oxidized forms of the complexes are indicative of the ligand-centered radicals in the oxidized derivatives.

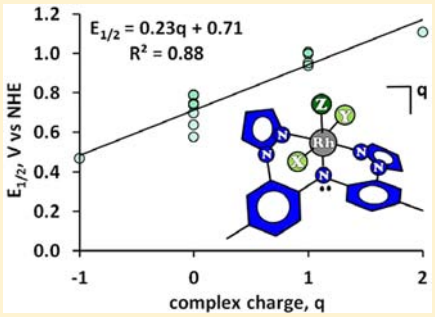

INTRODUCTION

An emergent area of contemporary research interest centers on the development and study of metal complexes that contain redox-active ligands for potential applications that span from molecular electronics to catalysis.[1] One of the main goals of research in this area is to exploit the redox-active ligand as an "electron reservoir" to promote unusual chemical reactivity,[2] to negotiate electron/hole transfer processes in molecular wires,[3] or to identify new examples of valence tautomerism.[4] In each area, an intimate knowledge of the electrochemical properties of the metal-bound redox-active ligand and the spectroscopic properties of the reduced and oxidized forms of a complex are vital for advancement. For systematic explorations in this context, it is desirable that a given redox-active ligand is easily accessed and contains simple synthetic handles to permit tuning of the electronic or steric environment about a bound metal. We recently reported on a new class of redox-active ligands related to bis(4-methyl-2-(1*H*-pyrazol-1-yl)phenyl)-amine, H(**L**), Figure 1 (where X = Z = Me; R = H), that possesses such characteristics.[5,6]

In tricarbonylrhenium(I) chemistry it was found that one-electron oxidation of $(^{R}ZX)Re(CO)_3$ gave a ligand-centered radical and that changing R- groups from hydrogen to alkyls caused ligand folding and enhanced ligand-centered reactivity.[5] By examining the carbonylrhodium(I) chemistry,[6] the electronic properties and reactivity of the ligands were found to be predictably tuned by varying the *para*-aryl substituents. Ligands with methyl substituents (Z and/or X = CH_3 in Figure 1) gave more electron rich carbonylrhodium(I) centers and

Received: April 13, 2012
Published: October 4, 2012

   dx.doi.org/10.1021/ic300772h | *Inorg. Chem.* 2012, 51, 10572−10580

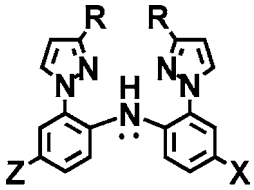

H(^{R}ZX)

Figure 1. Generic representation of redox-active ligands H(^{R}ZX). For this study, the ligand H(**L**) has R = H, Z = X = CH_3.

faster oxidative addition reactions with alkyl halides than when the ligand aryl arms possessed trifluoromethyl groups (Z and/or X = CF_3). While the trend in observed electronic properties of a series of related complexes with different substituents along the ligand periphery is understandable and predictable, the *magnitude* of changes in properties was not so easily predicted.

It is well-known that the empirical ligand additivity models offered by Bursten,[7] Pickett,[8] Lever,[9] Pombeiro,[10] and others[11] can be used to predict the electrochemical properties of a *metal-based* redox couple for complexes of the type $MX_nY_oZ_p$ with various numbers (*n*, *o*, *p*) and types of ligands (X, Y, Z). These models can also account for the known differences in the electronic properties of stereoisomers of a given complex. We were curious whether such models could be used to predict the oxidation potential for a *ligand-based* **L**/**L**$^{\cdot+}$ couple in a series of $LMX_nY_oZ_p$ complexes. For this purpose we chose to examine rhodium(III) complexes of the redox-active ligand (**L** = bis(4-methyl-2-(1*H*-pyrazol-1-yl)phenyl)amido) given the expected kinetic inertness of this metal's complexes and the apparent electrochemical reversibility of the **L**/**L**$^{\cdot+}$ couple in metal complexes of the ligand. Thus, we outline the synthesis of a convenient reagent for coordination chemistry of rhodium(III) complexes with this redox-active ligand, namely, $(NEt_4)[(\mathbf{L})RhCl_3]\cdot H_2O$, **2**·$H_2O$. On the basis of the results obtained from **2**·H_2O and the subsequent coordination complexes derived from this reagent, we also describe the relationship between the oxidation potential and the nature of the exogenous (X,Y,Z) ligands in $(\mathbf{L})RhX_nY_oZ_p$ complexes.

EXPERIMENTAL SECTION

The synthetic and computational details are given in the Supporting Information.

RESULTS AND DISCUSSION

Syntheses. As summarized in Scheme 1, the reaction between the protonated ligand H(**L**) and commercial rhodium(III) chloride hydrate in refluxing ethanol lead to the formation of a golden-beige insoluble solid that analyzed as $[H(\mathbf{L})]RhCl_3$, **1**. Complex **1** is insoluble in most organic solvents with the exception of Brønsted basic amines, solvents that react with **1**. For instance, dissolution of **1** in pyridine at room temperature caused deprotonation of the ligand and to give deep-green crystals of $(Hpy)[(\mathbf{L})RhCl_3]\cdot py$, **A**, after vapor diffusion of Et_2O into the reaction mixture (vide infra). Inspired by this observation, we found that deprotonation of **1** with $(NEt_4)(OH)$ in MeOH afforded high yields of the deep-green complex, $(NEt_4)[(\mathbf{L})RhCl_3]\cdot H_2O$, **2**·$H_2O$, an easily handled and synthetically useful reagent. Anhydrous **2** can be obtained after crystallization from CH_2Cl_2:hexanes and by taking precautions to avoid exposure to atmospheric moisture. Since we found the ensuing coordination chemistry of this complex to be insensitive to the presence (or absence) of the water of hydration, we chose to work with the hydrate **2**·H_2O under normal laboratory conditions rather than with anhydrous **2** under anaerobic conditions.

The reactions in Schemes 2−4 represent optimized routes to the various rhodium(III) complexes used in this study. Thus, heating a solution of **2**·H_2O and 5 equiv of either pyridine, triethylphosphine, or pyrazine in $CHCl_3$ at 60 °C for 16 h, gave mixtures that contained the highest yields (ca. 40−60%) of the appropriate *trans*-$(\mathbf{L})RhCl_2(py)$, *trans*-**3**, *trans*-$(\mathbf{L})RhCl_2(PEt_3)$, *trans*-**4**, or *trans*-$(\mathbf{L})RhCl_2(pyz)$, *trans*-**5**, respectively, products that are easily separated from unreacted **2**·H_2O, $[(\mathbf{L})Rh(py\text{ or }PEt_3)_2Cl](Cl)$ and other byproduct by chromatography. Heating solutions of either *trans*-**3**, *trans*-**4**, or *trans*-**5** in $C_2H_2Cl_4$ at 100 °C (for kinetic studies, or heating at reflux for preparative work) caused conversion to the appropriate *cis*-isomer (right of Scheme 2). In the case of **3**, the isomerization performed at 100 °C proceeds cleanly but stops after a 91:9 equilibrium mixture of *cis*-**3**:*trans*-**3** is attained. For **5** the 100 °C isomerization stops after a 90:10 equilibrium mixture of *cis*-**5**:*trans*-**5** is attained but there were small amounts (<10%) of another unidentified byproduct formed (Supporting Information, Figure S10). The re-isomerization of *cis*-**3** or *cis*-**5** to the respective *trans*- isomers was achieved by irradiation of dichloromethane solutions with high-intensity visible light. With **4**, the *trans*- isomer is completely consumed upon heating to 100 °C in $C_2H_2Cl_4$ but the isomerization to *cis*-**4** was not clean; there are at least two other unidentified byproduct formed during the conversion. In all cases it is possible to isolate at least small quantities of the pure *cis*- isomer by flash chromatography,[12] which indicates a rather high activation barrier to isomerization. In fact, isomerization of **3** or **4** did not occur in lower boiling solvents such as $CHCl_3$ (bp 61 °C) or THF (bp = 65 °C). On the other hand, the *trans*- to *cis*-isomerization of **5** was 50% complete in boiling $CHCl_3$ after 15 h. By examining initial rates of conversion spectroscopically (by monitoring the disappearance of the *trans*- isomer and/or the

Scheme 1. Preparation of $(NEt_4)[(\mathbf{L})RhCl_3]$, 2

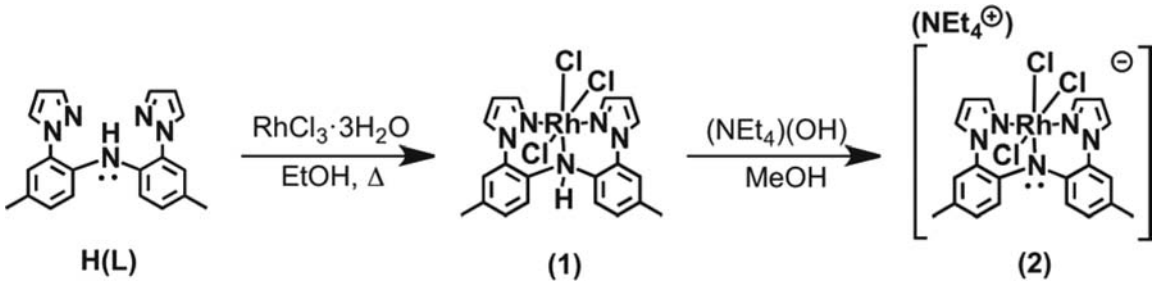

dx.doi.org/10.1021/ic300772h | *Inorg. Chem.* 2012, 51, 10572−10580

Scheme 2. Preparation and Isomerization of (L)$RhCl_2$(py), 3, (L)$RhCl_2$(PEt_3), 4, and (L)$RhCl_2$(pyz), 5

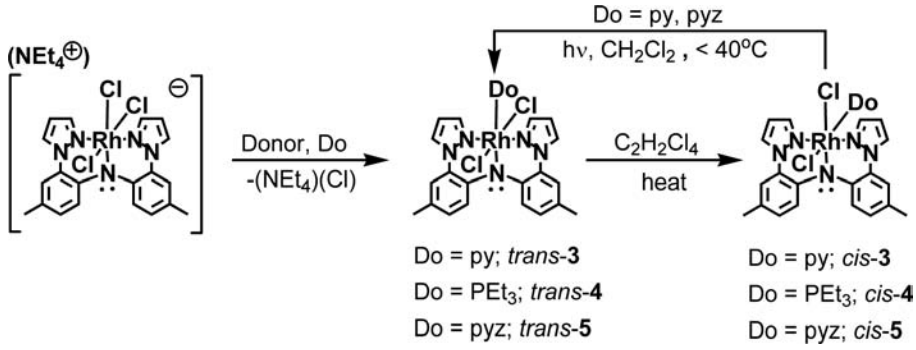

Scheme 3. Synthetic Routes to Monocationic $[(L)RhCl(donor)_2]^+$ Species, 6, 8, and 9

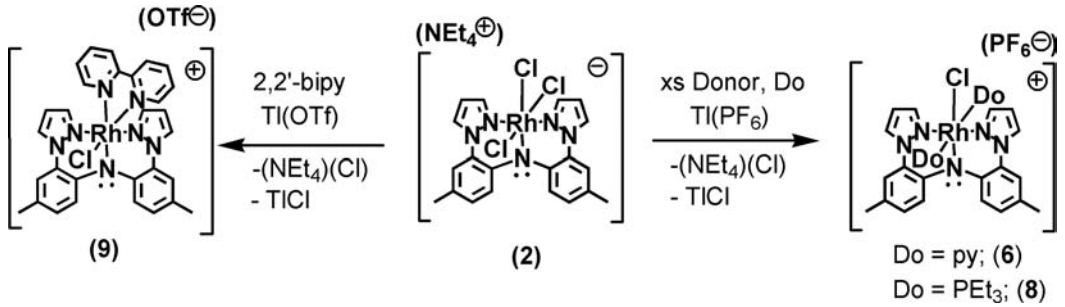

Scheme 4. Preparation of $[(L)Rh(ttpy)](OTf)_2$, 10

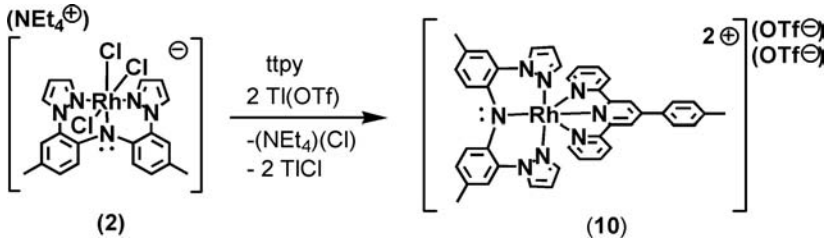

appearance of *cis*- isomer), the isomerization in $C_2H_2Cl_4$ at 100 °C was found to be first order in *trans*- isomer with $t_{1/2}$ on the order of 0.25 h for *trans*-**5**, 2.0 h for *trans*-**3**, and 6.6 h for *trans*-**4**. The unique ability for *trans*-**5** to undergo isomerization in a low-boiling solvent ($CHCl_3$) compared to *trans*-**3** or *trans*-**4** is likely due to the relatively poor donating ability of pyz versus py or PEt_3 to rhodium(III).[12,13] The relative donor ability of the Lewis base is also manifest in the electrochemistry of this series of complexes (vide infra). For the isomerization of *trans*-**3**−**5**, a rate-limiting step of dissociation of the *trans*- Lewis base, D_o, (rather than dissociation of a chloride) is suggested by five lines of evidence: (*i*) the relatively high activation barrier necessary to begin isomerization; (*ii*) the isomerization reaction is slowest for the strongest σ-donating group (PEt_3); (*iii*) the observation of free D_o in the ^1H NMR spectrum during isomerization, (*iv*) for a given complex $LRhCl_2(D_o)$, the rate of isomerization is independent of the presence (or absence) of added base, D_o, and; (*v*) in a competition experiment monitored by ^1H NMR spectroscopy,[12] *trans*-**3** and *cis*-**3** are formed within 10 min of heating a solution of *trans*-**5** and excess pyridine at 100 °C. In the latter reaction, *trans*-**5** was completely consumed within 30 min, trace *cis*-**5** formed during the first 10 min, and was barely detectable after 6 h. The ^1H NMR spectrum was mainly a superposition of *trans*-**3**, *cis*-**3**, free pyrazine, and excess pyridine, and no signals attributable to a species such as $[(L)Rh(py)(pyz)(Cl)](Cl)$ were found.

The reaction between **2**·H_2O, an excess of either pyridine or triethylphosphine, and 1 equiv of $Tl(PF_6)$ as a halide abstracting agent in refluxing pyridine or acetonitrile (in the PEt_3 case) produced high yields of the appropriate $[(L)RhCl(py)_2](PF_6)$, **6**, or $[(L)RhCl(PEt_3)_2](PF_6)$, **8**, Scheme 3. The NEt_4Cl byproduct of the reactions is easily removed by washing the organic soluble components with water. The reaction of *trans*-**3** with excess PPh_3 and 1 equiv of $TlPF_6$ afforded $[(L)Rh(py)(PPh_3)Cl](PF_6)$, **7**, that has the chloride *trans*- to the amido. Single-crystal X-ray diffraction and NMR spectral data (vide infra) indicate a *trans*- disposition of monodentate Lewis donors in **6** and **8**. A *cis*- arrangement of ligands can be enforced using the chelating 2,2′-bipy as the donor (and Tl(OTf) as a halide abstracting agent) to give $[(L)RhCl(bipy)](OTf)$, **9**. Similarly, the reaction between **2**·H_2O, the tridentate ttpy ligand, and 2 equiv of Tl(OTf) afforded $[(L)Rh(ttpy)](OTf)_2$, **10**, as in Scheme 4. Interestingly, attempts to prepare $[(L)Rh(donor)_3](PF_6)_2$ where donor = py or PEt_3 were unsuccessful even when using a large excess of pyridine or PEt_3 and thallium(I) salts. Thus, the chelate effect appears to facilitate the abstraction of the third halide ligand of **2**·H_2O.

dx.doi.org/10.1021/ic300772h | *Inorg. Chem.* 2012, 51, 10572−10580

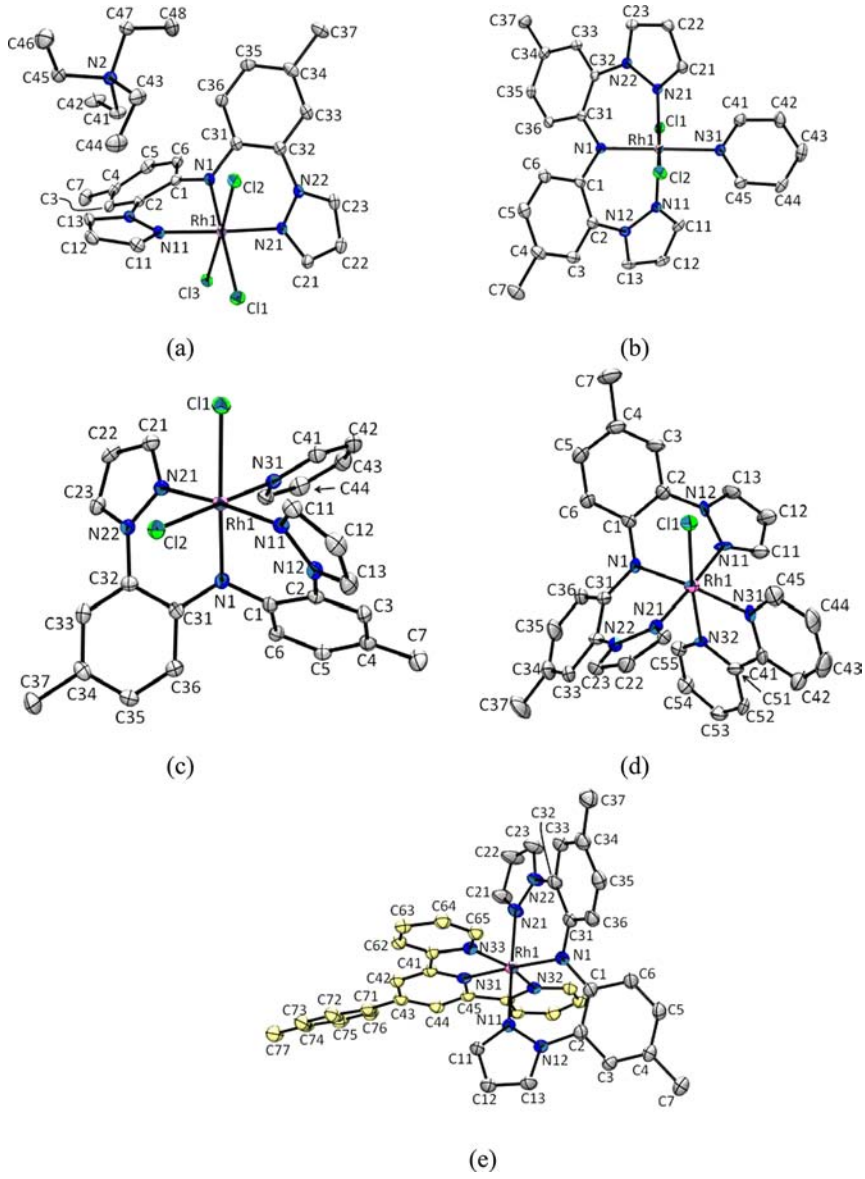

Figure 2. Structures of (a) $(NEt_4)[(\mathbf{L})RhCl_3]$, (b) *trans*-$(\mathbf{L})RhCl_2(py)$, (c) *cis*-$(\mathbf{L})RhCl_2(py)$; (d) $[(\mathbf{L})RhCl(bipy)]^+$, (e) $[(\mathbf{L})Rh(ttpy)]^{2+}$. Thermal ellipsoids are drawn at the 50% probability level. Hydrogen atoms, solvent molecules, and anions have been omitted for clarity. Thermal ellipsoids are drawn at the 50% probability level. Hydrogen atoms, solvent molecules, and anions have been omitted for clarity.

Structures. Crystals of $(Hpy)[(\mathbf{L})RhCl_3]\cdot py$ (**A**), **2**, *trans*-**3**, *cis*-**3**, *trans*-**4**, and **7**−**10** suitable for single crystal X-ray diffraction were obtained. Views of the structures of **2**, *trans*-**3**, *cis*-**3**, **9**, and **10** are given in Figure 2 while others are provided in the Supporting Information. Selected bond distances and angles for all are given in Table 1. In each complex, the anionic pincer-type ligand has a planar amido nitrogen (indicated by the 360° sum of the angles about nitrogen N1) and binds each octahedral rhodium(III) center in a meridional *N,N,N*-coordination mode. The average Rh−N(pyrazolyl), $Rh-N_{pz}$, bond distances are in the range of 2.01 to 2.03 Å, which mirrors previous findings for (**L**)Rh(Et or I)(CO)(I) and $[(\mathbf{L})Rh(I)(\mu\text{-}I)]_2$ complexes.[6] The amido Rh−N1 (or $Rh-N_{Ar}$) bond distance shows greater variability than $Rh-N_{pz}$ and appears to depend mainly on the substituent disposed *trans*- to the amido nitrogen. Of the series of complexes listed in Table 1, the longest Rh−N1 bond of 2.064(2) Å is found for *trans*-**4** with the strongest σ-donor, PEt_3, that is linearly disposed from the amido group, N1−Rh1−P1 = 178.23(6)°. The shortest Rh−N1 bond of 2.000(2) Å is found for *trans*-**3** with a pyridyl *trans*- to the amido. In this derivative, the pyridyl ring and the amido fragment C1N1(Rh)C31 are nearly coplanar with a C1C31−C41C45 torsion angle of 1°. In this geometry it is expected that the π (and π^*) orbitals of the pyridyl would be in full conjugation with the filled π-orbitals on the amido fragments and rhodium (vide infra). In contrast, the chelating nature of the bipy and ttpy ligands forces the *trans*-disposed pyridyl ring of the multidentate ligand to be twisted out of conjugation with the amido fragment C1N1(Rh)C31; the C1C31−C41C45 torsion angle is 44° for **9** and is 46° for **10**. In these latter cases, the Rh−N1 distances of 2.017(9) Å for **9** and 2.014(3) Å for **10** are longer than in *trans*-**3**. The corresponding Rh−N31, or $Rh-N_{py}$, bond distances involving the ring *trans*- to the amido decreases from 2.097(2) Å for *trans*-**3**, 2.064 Å for **9**, and 1.969(3) Å for **10**, which likely reflects the effect of increasing charge on the complex and possibly the increasing π-acceptor

dx.doi.org/10.1021/ic300772h | *Inorg. Chem.* 2012, 51, 10572−10580

Table 1. Selected Bond Distances (Å) and Angles (deg) for the New Rhodium(III) Pincer Complexes[a]

	complexes								
	A	**2**	*trans*-**3**	*cis*-**3**	*trans*-**4**	**7**	**8**	**9**	**10**
				Distances (Å)					
Re−N_{Ar}	2.010(2)	2.017(1)	2.000(2)	2.013(2)	2.064(2)	2.023(3)	2.042(4)	2.017(9)	2.014(3)
Re−N_{pz}[a]	2.010(2)	2.013(2)	2.016(2)	2.015(2)	2.033(2)	2.018(3)	2.026(4)	2.023(9)	2.016(3)
Re−N_{py}[a]			2.097(2)	2.065(2)		2.140(3)		2.066(9)	2.033(3)
Re−P					2.346(1)	2.3484(8)	2.413(1)		
Re−Cl_{ax}[b]	2.3551(7)	2.3481(4)	2.3418(5)	2.3398(7)	2.3481(6)			2.332(3)	
Re−Cl_{eq}[c]	2.4056(6)	2.3937(4)		2.3903(7)		2.3713(7)	2.379(2)		
				Angles (deg)					
N11−Re−N1	87.77(9)	88.41(6)	88.00(8)	88.99(10)	84.25(8)	88.22(10)	88.7(2)	88.5(4)	89.23(11)
N21−Re−N1	90.25(9)	87.60(6)	87.94(8)	87.43(10)	83.63(8)	89.52(10)	88.8(2)	88.7(4)	88.54(11)
N31−Rh−N1			179.21(7)	87.89(10)		88.88(10)		175.3(4)	178.02(11)
N31−Rh−N32								80.3(4)	80.25(12)
N32−Rh−N33									160.39(11)
pz-aryl	29.5	32.0	31.9	33.7	40.9	30.4	34.9	30.2	26.8
RhN−NC_{ipso}[d]	6.4	6.9	8.1	8.1	5.9	10.8	13.6	2.6	7.2

[a]In cases where more than one of the same type of atom or crystallographically independent molecule is present, an average value is reported. [b]*cis*- to amido N1 atom. [c]*trans*- to amido N1 atom. [d]Absolute value of torsion angle.

character of the exogeneous ligands. It is also known that the constrained geometry associated with terpyridyl group gives rise to metal chelate complexes where the metal−nitrogen bonds to the central ring are ∼0.09 shorter than those involving the outer rings.[14] The Rh−N_{py} bond distance 2.065(2) Å in *cis*-**3** is shorter than that in *trans*-**3**. The cation in **9** displays statistically identical Rh−N_{py} bond distances of 2.067(9) and 2.065(9) Å. The Rh−Cl bond distances across the entire series of complexes display a strong *trans*- influence with the chloride situated *cis*- to the amido being much shorter than a chloride *trans*- to the amido, regardless of the charge on the complex.

Solution Characterization. The ^{1}H, ^{13}C, and ^{31}P NMR spectra are in general agreement with expectations based on the idealized symmetry and solid-state structures of the complexes. With the exception of **7**, which had several regions of overlapping multiplet resonances in the aromatic regions that hindered analysis, full assignments of resonances in the ^{1}H NMR spectra could be made by analysis of 1D spectrum and 2D (DQCOSY and NOESY) spectra. Full details and discussion of data are provided in the Supporting Information.

The rhodium(III) complexes of the bis(4-methyl-2-(1*H*-pyrazol-1-yl)phenyl)amido ligand are intensely colored species like the previously reported carbonylrhodium(I) (d^8), organorhodium(III) (low spin d^6), or even the tricarbonylrhenium(I) (low-spin d^6) counterparts.[5] Table 2 summarizes data from electronic spectroscopic measurements of **2**−**10** in CH_2Cl_2; the data acquired in CH_3CN are found in the Experimental section (in the Supporting Information). All complexes exhibit high-intensity bands below 300 nm ($\varepsilon > 10^4$ M^{-1} cm^{-1}) that are likely $\pi-\pi^*$ transitions, on the basis of energy and intensity considerations. Each complex also exhibits a medium-intensity band (ε ca. 10,000−20,000 M^{-1} cm^{-1}) centered in a narrow range of 320−350 nm that is likely an n−π^* transition given its rather invariant energy range and intensity across the series of complexes as well as its similarity with the band found for solutions of the free ligand, H(**L**) (λ_{max} = 320 nm, ε = 22,500 M^{-1} cm^{-1}). The lower energy, visible bands (λ_{max} > 350 nm) are likely for ligand-to-metal charge transfer (LMCT) and/or ligand-to-ligand charge transfer (LLCT) transitions, as suggested by a comparison of their energies and intensities relative to related complexes[15] and by

Table 2. Summary of Electronic Absorption Spectra Data for Complexes 2−10 in CH_2Cl_2

compound	λ, nm (ε, M^{-1} cm^{-1})
2:	241 (55,700), 348 (13,800), 382 (7,600), 416 (8,700), 590 (1,500), 720 sh (500)
trans-**3**·CH_2Cl_2:	239 (63,800), 339 (12,600), 376 (9,900), 405 (10,400), 592 (1,040)
cis-**3**:	246 (56,600), 339 (13,700), 362sh (9,000), 388 (8,900), 519 (2,400)
trans-**4**:	244 (56,700), 286 (18,100), 339 (13,600), 378 (6,500), 412 (8000), 455 (3,900), 570 (900)
cis-**4**:	248 (61,900), 345 (12,300), 398 (7,600), 512 (2,700), 658 (1,150), 725 sh (980)
trans-**5**:	241 (51, 000), 337 (9,200), 379 (6,400), 407 (8,100), 500 sh (1,700), 600 (810)
cis-**5**:	243 (37,500), 334 (9,100), 371 (5,100), 393 (5,600), 503 (1,200)
6:	248 (60,700), 328 (14,500), 365sh (8,100), 499 (2,900)
7:	245 (92, 000), 326 (17,900), 391 (9,800), 502 (2,100)
8:	253 (54,900), 344 (14,300), 385 (7,100), 510 (3,000)
9:	242 (69,900), 327 (14,900), 364sh (8,500), 390 (8,900), 443 (2800), 510sh (3,000), 555 (1100)
10:	240 (53,600), 312 (22,400), 320 (22,700), 345 (19,900), 362 (20,900), 430 (2500), 645 (1300)

theoretical calculations (TD-DFT, see Supporting Information for full details). The frontier orbitals for two representative complexes *trans*-**3** and *trans*-**4** are shown in Figure 3. The highest occupied molecular orbital (HOMO) for all complexes is a π_L orbital (pi-lone-pair orbital, as per Kasha's convention[16]) on the pincer-type ligand with a small π-antibonding contribution from a metal d-orbital. For pyridyl or poly(pyridyl)-containing complexes **3**, **6**, **7**, **9**, and **10**, the π^* orbitals on pyridyl rings constitute the lowest unoccupied molecular orbital (LUMO). Thus, the lowest energy band (HOMO−LUMO transition) for each of these four complexes is LLCT in character. For the other complexes such as **2**, **4**, and **8**, the LUMO is a σ^* orbital with pronounced metal character. In these latter cases, the lowest energy transition is LMCT in nature. For all complexes, the subsequent higher energy visible bands involve transitions between different HOMO($-M$) (M = 0−3) and LUMO($+N$) (N = 0−4) levels that represent the gamut of various LMCT or LLCT transitions involving ligand

dx.doi.org/10.1021/ic300772h | *Inorg. Chem.* 2012, 51, 10572−10580

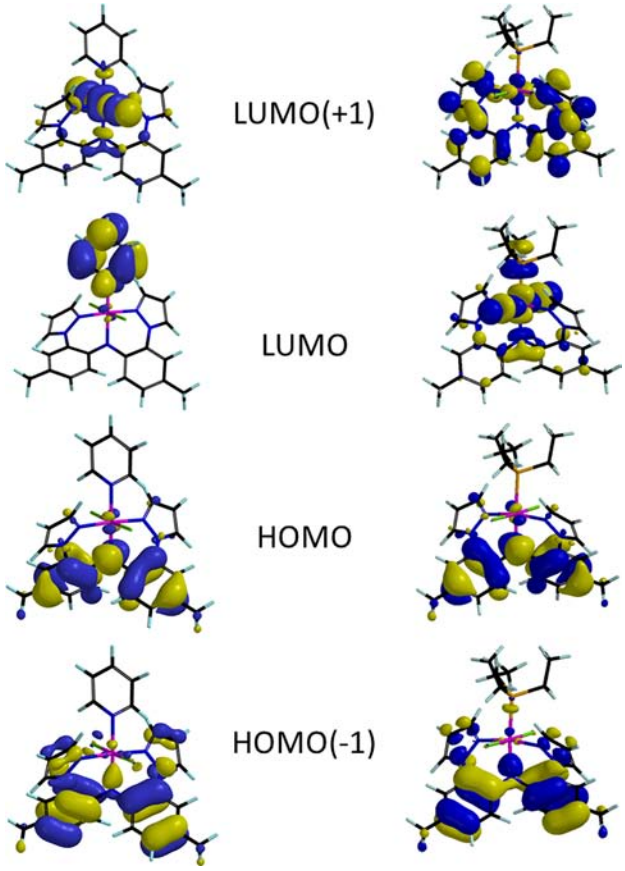

Figure 3. Frontier orbitals for *trans*-**3** and *trans*-**4** from DFT calculations (B3LYP/LACVP).

(**L**) and supporting ligand orbitals, as summarized in the Supporting Information. The d-d transitions are not observed as these expectedly weak-intensity transitions are likely obscured by the other, more intense bands. As with many other transition metal complexes,[17] the dramatic color difference between different stereoisomers of (**L**)$RhCl_2(D_o)$ is due to only to small differences in the electronic spectra, exemplified for *trans*-**3** and *cis*-**3** in Figure 4. The lowest energy absorption band in spectrum of *trans*-**3** for the LLCT transition is centered in the orange region and extends further into the red than that in *cis*-**3** which is centered in the green region and extends into the orange-red. This band, in part, gives rise to the

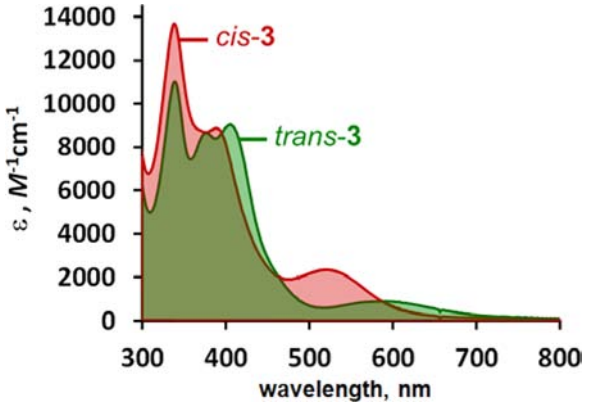

Figure 4. Electronic absorption spectrum of *trans*-**3** (green) and *cis*-**3** (red) in CH_2Cl_2.

green color for the former and the red-brown color of the latter. The second lowest energy band near 400 nm in the spectrum of *trans*-**3** is split whereas only one band is found in *cis*-**3**. This observation is in accord with the general observation of greater tetragonal splitting of *trans*- versus *cis*- isomers found in spectra of coordination complexes with local MX_4Y_2 kernels.[18]

Cyclic Voltammetry. The electrochemistry of the various complexes was investigated and a summary of findings from cyclic voltammetry experiments is given in Table 3. A

Table 3. Summary of Electrochemical Data for 2−10 and Reference Complexes[a]

	oxidation	reduction
compound	$E_{1/2}$[b] (ΔE, mV)[c]	$E_{1/2}$ (ΔE, mV)[c]
2·H_2O	+0.27 (182)	not observed
trans-**3**	+0.44 (231)	E_{pf} = −1.56 (irrev.)
cis-**3**	+0.55 (177)	E_{pf} = −1.20 (irrev.)
trans-**4**	+0.38 (135)	E_{pf} = −1.57 (irrev.)
cis-**4**	+0.54 (104)	E_{pf} = −0.88 (irrev.)
trans-**5**	+0.50(152)	E_{pf} = −1.46 (irrev.)
cis-**5**	+0.59(150)	E_{pf} = −1.51 (irrev.)
6	+0.81 (227)	E_{pf} = −1.56 (irrev.)
7	+0.75 (124)	E_{pf} = −1.40 (irrev.)
8	+0.80 (140)	E_{pf} = −1.53 (irrev.)
9	+0.74 (182)	−1.12 (152), E_{pf} = −1.45 (irrev.)
10	+0.91 (152)	−0.77 (145), E_{pf} = −1.30 (irrev.)
(**L**)RhMe(CO)(I)[d]	+0.79 (136)	not observed
ferrocene	+0.41 (190)	not observed

[a]Samples as 0.1 mM solutions in CH_2Cl_2 with 0.1M NBu_4PF_6 as a supporting electrolyte. [b]Average value from scan rates of 50, 100, 200, 300, 400, and 500 mV/s, V versus Ag/AgCl. [c]For a scan rate of 200 mV/s. [d]See ref 6.

representative set of voltammograms for *trans*-**3** is given in Figure 5. Each complex shows a quasi-reversible ($E_{p,a}$-$E_{p,c}$ > 59

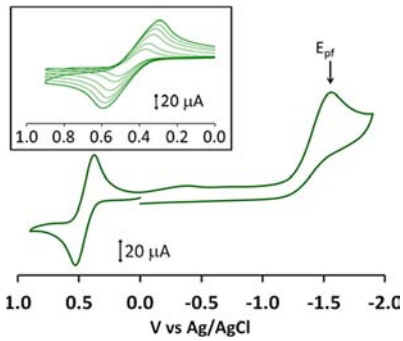

Figure 5. Cyclic voltammogram (300 mV/s) obtained for *trans*-**3** in CH_2Cl_2 with NBu_4PF_6 as a supporting electrolyte. Inset: Oxidation waves obtained at 50 (innermost plot), 100, 200, 300, 400, and 500 (outermost plot) mV/s. The vertical arrow near −1.6 V in the voltammogram is the E_{pf} cited in Table 3.

mV and increases with scan rate, see inset of Figure 5), one-electron, ligand-based oxidation wave at potentials that depend mainly on the overall charge of the complex and to a lesser extent on the nature of the exogenous supporting ligands. That is, **2**·H_2O, with an anionic complex, has the lowest oxidation potential at +0.27 versus Ag/AgCl. The charge-neutral rhodium(III) complexes **3**−**5** are at least +0.1 V more stable

dx.doi.org/10.1021/ic300772h | *Inorg. Chem.* 2012, 51, 10572−10580

than **2**·H_2O with respect to oxidation. In these latter complexes the oxidation potentials are dictated by the ligand *trans*- to the amido group where *trans*-**4**, with a strong σ-donating PEt_3 group, exhibits a lower oxidation potential (+0.38 V) than *trans*-**3** (+0.44 V) or *trans*-**5** (+0.50 V). For the *cis*- isomers of **3**−**5** that have a chloride *trans*- to the amido, the oxidation potential falls into a narrow range of +0.54 to +0.59 V. The same trend found in the *trans*- series applies for the *cis*- series where the complex with the strongest σ- donor is easiest to oxidize: *cis*-**5** (+0.59 V), *cis*-**3** (+0.55 V), *cis*-**4** (+0.54).

The chelating dipyridyl derivative **9** is detectably more electron-rich (E_{ox} = +0.74 V) than **6** (E_{ox} = +0.81 V) with two *trans*- disposed pyridine rings. The dicationic ttpy derivative in **10** is the most difficult to oxidize (+ 0.91 V) of the series, as might be expected based from Coulombic considerations. Each complex also shows an irreversible, presumably, metal-based reduction at E_{pf} values equal to or more negative than −1.2 V versus Ag/AgCl. A quasi-reversible, one-electron, polypyridyl-based reduction wave is found at −1.12 V for **9** and −0.77 V for **10**. The HOMO−LUMO energy gaps of 1.86 eV (or 667 nm) for **9** and 1.68 eV (or 738 nm) for **10** from electrochemical experiments are close to those obtained from UV−visible spectroscopic experiments (692 nm for **9** and 747 nm for **10**) by using the onsets of the low energy transitions, which lends support to the LLCT assignment of the lowest-energy visible band in the electronic spectrum.

Chemical Oxidations. Given the electrochemical quasi-reversibility of the oxidation waves for the complexes reported above, the chemical oxidations of *trans*-**3**, *cis*-**3**, and **8** were investigated to probe the nature of the resulting doublets. In each case, the one-electron oxidation gave paramagnetic complexes (μ_{eff} ca. 1.8 μ_B) that were ligand-centered radicals based on structural and spectroscopic studies. The experimental findings were also supported by the results of theoretical calculations. Spectrophotometric redox titrations were performed by adding substoichiometric amounts of *trans*-**3**, *cis*-**3**, or **8** in CH_2Cl_2 to solutions of the moderately strong organic cation radical oxidant, 9,10-dimethoxyocta-hydro-1,4:5,8-dimethanoanthracenium hexachloroantimonate, (CRET)($SbCl_6$) (ε_{518} = 7300 M^{-1} cm^{-1}, $E_{1/2}$ = +1.09 versus Ag/AgCl).[19] As shown for *trans*-**3** in Figure 6, the characteristic π- radical bands

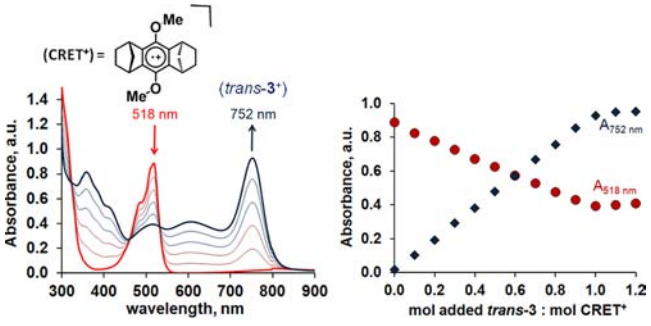

Figure 6. Spectrophotometric redox titration of *trans*-**3** with (CRET)($SbCl_6$) in CH_2Cl_2.

at λ = 752, 606, 517 nm for HOMO(−*N*) (*N* = 0−3) to singly occupied molecular orbital (SOMO) transitions of the oxidized (metal-bound) ligand grow at the expense of the band at λ_{max} = 518 for (CRET)($SbCl_6$) until an equimolar ratio of oxidant:*trans*-**3** is reached, verifying the one-electron nature of the oxidation. Similar results were found for the other two complexes. Synthetic scale oxidations used either (CRET)-($SbCl_6$) or (NO)($SbCl_6$) as the oxidant. Electron paramagnetic resonance (EPR) spectra for ambient temperature and frozen (5 K) CH_2Cl_2 solutions of the bulk powders showed isotropic signals with g-factors of 2.010 for each (*trans*-**3**)$^+$ and (*cis*-**3**)$^+$ and of 2.013 for (*trans*-**8**)$^{2+}$. These g-factor values are near the free electron value and are indicative of ligand centered radical; the oxidized species are unlikely to be mainly metal-centered radicals since low-spin Rh(IV) is typically EPR silent at ambient temperature.[20]

X-ray quality crystals of each oxidized derivative could be grown by diffusing hexanes or toluene into small-scale reaction mixtures in CH_2Cl_2. Figure 7 shows overlays of the structures of the isomers of **3** and their oxidized forms, (**3**)$^+$ while the associated metrical data are found in Table 4. The structural overlay of **8**$^+$ and **8**$^{2+}$ along with data and discussion are given in the Supporting Information. One of the main differences between the structures of the reduced and oxidized forms of the complexes is manifest in changes in the coordination environment about rhodium. In particular, the distances along the N_{Ar}−Rh−X (X = Cl1 or N31) vector decrease upon oxidation. Such changes would be expected if an antibonding orbital (from dπ-pπ interactions) were to become depopulated upon oxidation. The HOMO of *trans*-**3** left of Figure 3 and the SOMO of (*trans*-**3**)$^+$ and similar MO diagrams for the other complexes (Supporting Information) indeed show such interactions. Within the ligand-centered HOMO of each complex, there are π-antibonding interactions between atoms corresponding to bonds A, A′, C, C′, F, and F′ and π-bonding interactions corresponding to bonds B, B′, G, and G′, as per the labeling diagram to the right of Figure 7. Thus, the depopulation of the HOMO by oxidation should lead to a shortening of the former bonds and a lengthening in the latter bonds (B, B′, G, and G′). In general, such changes are observed but in many cases these changes upon oxidation are at the borderline of being or are not statistically significant. The most significant changes in ligand bonds of *trans*-**3** upon oxidation are found for bond F′ (shortened by 0.008 Å) and bond G′ (lengthened by 0.018 Å); the shortening of bonds C and C′ (Table 4) are at the borderline of statistical significance. Similarly for *cis*-**3**, bond F′ (shortened by 0.014 Å) and bond G′ (lengthened by 0.011 Å) show significant changes upon oxidation. For **8**, bonds C and F′ show significant shortening, but changes in other ligand bond distances are statistically insignificant. Concomitant with bond distance changes upon oxidation, there is a detectable reduction in dihedral angles involving the aromatic and heterocyclic rings, leading to an overall increase in ligand planarity. Thus, the dihedral angle between mean planes of the pyrazolyl-ring and the tolyl-group to which it is bound reduces by 2−4° upon oxidation. The dihedral angle between mean planes of tolyl group arms either remains unchanged (compared to the average of three independent units of **8**) or reduces by up to 4° (for *trans*-**3**) upon oxidation. Such changes in the ligand framework lead to subtle, but difficult-to-rationalize, differences in the (RhN-NC) torsion angles, the so-called "pyrazolyl ring-twisting" that describes the "fit" of the ligand to the metal center.[21]

DISCUSSION

The discovery of the convenient new reagent (NEt_4)[(**L**)-$RhCl_3$]·H_2O, **2**·H_2O, has been central to the development of new rhodium(III) coordination chemistry involving the redox active bis(4-methyl-2-(1*H*-pyrazol-1-yl)phenyl)amido ligand, **L**.

dx.doi.org/10.1021/ic300772h | *Inorg. Chem.* 2012, 51, 10572−10580

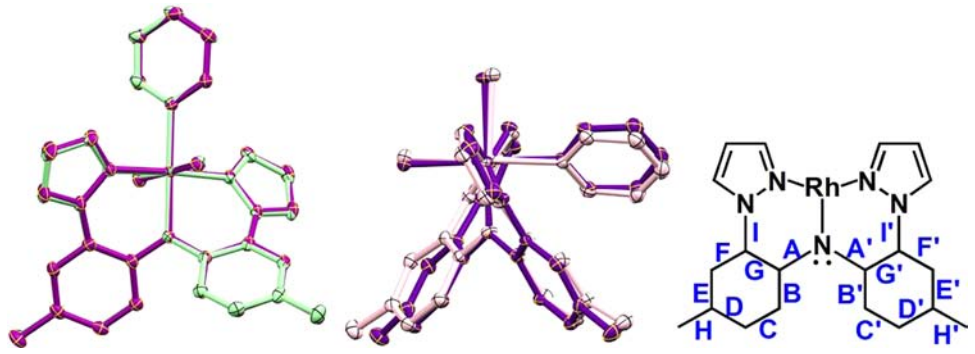

Figure 7. Left: Thermal ellipsoid plots (50% probability level) of *trans*-**3**, pale green, and (*trans*-**3**)$^+$, magenta, overlaid at the least-squares minimum mean position of five common atoms Rh, N_{pz}, and N_{py} and N_{Ar}; Center: Similar plot of *cis*-**3**, pale pink, and (*cis*-**3**)$^+$, violet, but overlaid at four atoms Rh, N_{pz}, and N_{Ar}; Right: Labeling diagram used for ligand bonds in Table 4.

Table 4. Comparison of Bond Distances and Angles in Isomers of 3 and (3)$^+$

	trans-**3**	(*trans*-**3**)$^+$	Δ^b	*cis*-**3**	(*cis*-**3**)$^+$	Δ^b
			Bond Distances (Å)			
Rh−Cl1	2.3425(5)	2.3318(8)	*−0.0107*	2.3903(7)	2.3446(9)	*−0.0457*
Rh−Cl2	2.3411(5)	2.3413(8)	*+0.0002*	2.3398(7)	2.3266(9)	*−0.0132*
Rh−N1	2.000(2)	1.985(2)	*−0.015*	2.013(2)	2.000(3)	*−0.013*
Rh−N11	2.012(2)	2.007(2)	*−0.005*	2.014(2)	2.024(3)	*+0.010*
Rh−N21	2.020(2)	2.019(2)	*−0.001*	2.015(2)	2.016(3)	*+0.001*
Rh−N31	2.097(2)	2.071(2)	*−0.026*	2.065(2)	2.073(3)	*+0.008*
			Ligand Bond Label[a]			
A	1.386(3)	1.384(4)	*−0.002*	1.384(4)	1.389(5)	*+0.005*
A′	1.386(3)	1.386(4)	*0.000*	1.393(4)	1.391(5)	*−0.002*
B	1.404(3)	1.410(4)	*+0.006*	1.401(4)	1.407(5)	*+0.006*
B′	1.414(3)	1.406(4)	*−0.008*	1.406(4)	1.403(6)	*−0.003*
C	1.381(3)	1.377(4)	*−0.004*	1.382(4)	1.381(6)	*−0.001*
C′	1.378(3)	1.374(4)	*−0.004*	1.385(4)	1.385(6)	*0.000*
D	1.391(3)	1.402(5)	*+0.009*	1.395(4)	1.398(6)	*+0.003*
D′	1.399(4)	1.396(4)	*−0.004*	1.398(4)	1.399(6)	*+0.001*
E	1.384(3)	1.385(4)	*+0.001*	1.383(4)	1.396(6)	*+0.013*
E′	1.387(4)	1.393(4)	*+0.005*	1.387(4)	1.389(6)	*+0.002*
F	1.396(3)	1.389(4)	*−0.007*	1.401(4)	1.387(5)	*−0.014*
F′	1.393(3)	1.385(4)	*−0.008*	1.393(4)	1.398(5)	*+0.005*
G	1.408(3)	1.413(4)	*+0.005*	1.405(4)	1.416(5)	*+0.011*
G′	1.402(3)	1.420(4)	*+0.018*	1.407(4)	1.408(5)	*+0.001*
H	1.509(3)	1.505(4)	*−0.004*	1.509(4)	1.502(6)	*−0.007*
H′	1.506(3)	1.502(4)	*+0.004*	1.498(4)	1.501(6)	*+0.003*
I	1.432(3)	1.421(4)	*−0.011*	1.431(4)	1.426(5)	*−0.005*
I′	1.433(3)	1.416(4)	*−0.017*	1.426(4)	1.419(5)	*−0.007*
			Dihedral and Torsion Angles (deg)			
Pz-tol	29.71	26.22	*−3.49*	32.05	27.60	*−4.45*
Pz-tol′	34.06	33.35	*−0.71*	35.29	29.83	*−5.46*
Tol-tol	69.04	64.27	*−4.77*	64.21	62.27	*−1.94*
|RhN-NCl	4.18	0.11	*−4.07*	2.99	7.15	*−4.16*
|(RhN-NC)′|	12.04	9.47	*−2.54*	13.12	15.60	*+2.48*

[a]See right of Figure 7 for labeling diagram of ligand bonds. [b]Δ = oxidized distance − nonoxidized distance.

Charge-neutral, mono- and dicationic complexes can be easily prepared from **2**·H_2O. For charge-neutral complexes (**L**)-$RhCl_2$(base), *trans*- isomers are metastable, kinetic products of the reaction between **2**·H_2O and Lewis bases. These *trans*-isomers are converted to the thermodynamically more stable *cis*- isomers by heating. All complexes are highly colored and electroactive. The electrochemistry associated with the rhodium(III) complexes is ligand-centered where the oxidation potential was found to span a remarkable range of 700 mV. Figure 8 reveals a decent linear correlation (R^2 = 0.88) in a plot of $E_{1/2}$ (vs NHE) versus charge for each of the first 13 complexes listed in Table 3. By considering the best fit line from linear regression analysis, $E_{1/2}$ (V vs NHE) = 0.23q + 0.71, the oxidation potentials for the seven charge-neutral complexes can be predicted to within ±105 mV. The variation in oxidation potentials for the seven charge-neutral complexes arises from the diversity of ligands disposed *trans*- to the redox-active diarylamido group, ligands which seem to most effectively control the electron density of **L**. For those derivatives with identical chloride groups *trans*- to the amido (as in *cis*-**3**, *cis*-**4**,

dx.doi.org/10.1021/ic300772h | *Inorg. Chem.* 2012, 51, 10572−10580

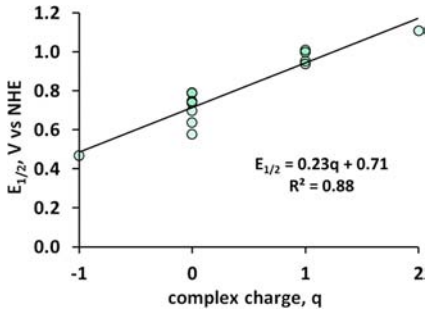

Figure 8. Plot of $E_{1/2}$ (vs NHE) versus charge, q, on various $[LRhXYZ]^q$ complexes.

and *cis*-**5**), the substituents *cis*- to the amido influence the oxidation potential. The variation in $E_{1/2}$ in the *trans*- versus *cis*-isomers of **3**−**5** indicate that the ligands *trans*- to the amido are about twice as effective at modulating oxidation potentials relative to the ligands disposed *cis*- to the amido. The oxidation potential of the four cations is quite accurately predicted from the best fit line from linear regression analysis since the observed values only span a range of 70 mV. As described in the Supporting Information, an empirical ligand additivity model can be developed to account for these small variations in redox potentials as a function of different ligands and stereochemistry of the metal complexes. However, such a model is much more cumbersome (and more tenuous) to use than a simple examination of $E_{1/2}$ versus complex charge, q, for predictions of redox potentials in known (and perhaps in hypothetical) rhodium(III) complexes of this ligand. Future manuscripts will explore the generality of these findings in transition metal chemistry and will describe the use of the (**L**)RhXYZ complexes in electron transfer reactions.

■ ASSOCIATED CONTENT

Ⓢ Supporting Information

Experimental procedures, analytical and spectral characterization data, computational details and molecular modeling coordinates, crystallographic information files (CIF), and expanded discussions of synthetic and NMR spectroscopic findings, and discussion of empirical ligand additivity model. This material is available free of charge via the Internet at http://pubs.acs.org.

■ AUTHOR INFORMATION

Corresponding Author

*E-mail: james.gardinier@marquette.edu.

Notes

The authors declare no competing financial interest.

■ ACKNOWLEDGMENTS

J.R.G. thanks the NSF (CHE-0848515) for financial support. We thank Dr. Brian Bennett (Medical College of Wisconsin) for assistance with EPR spectroscopic measurements.

■ REFERENCES

(1) (a) A recent forum issue on redox non-innocent ligands: *Inorg. Chem.* **2011**, *50*, 9737−9914. (b) Caulton, K. G. *Eur. J. Inorg. Chem.* **2012**, 435−443.

(2) (a) Lyaskovskyy, V.; de Bruin, B. *ACS Catal.* **2012**, *2*, 270−279. (b) Lu, F.; Zarkesh, R. A.; Heyduk, A. F. *Eur. J. Inorg. Chem.* **2012**, *2012*, 467−470.

(3) (a) Nishimori, Y.; Kanaizuka, K.; Kurita, T.; Nagatsu, T.; Segawa, Y.; Toshimitsu, F.; Muratsugu, S.; Utsuno, M.; Kume, S.; Murata, M.; Nishihara, H. *Chem.—Asian J.* **2009**, *4*, 1361−1367. (b) Olivier, C.; Kim, B.; Touchard, D.; Rigaut, S. *Organometallics* **2008**, *27*, 509−518. (c) Dong, T.-Y.; Lin, M.-C.; Chiang, M. Y.-N.; Wu, J.-Y. *Organometallics* **2004**, *23*, 3921−3930.

(4) By Kundu, N.; Maity, M.; Chatterjee, P. B.; Teat, S. J.; Endo, A.; Chaudhury, M. *J. Am. Chem. Soc.* **2011**, *133*, 20104−20107. Dei, A.; Sorace, L. *Appl. Magn. Reson.* **2010**, *38*, 139−153. Evangelio, E.; Ruiz-Molina, D. *C. R. Chim.* **2008**, *11*, 1137−1154. Sato, O.; Cui, A.; Matsuda, R.; Tao, J.; Hayami, S. *Acc. Chem. Res.* **2007**, *40*, 361−369.

(5) (a) Wanniarachchi, S.; Liddle, B. J.; Toussaint, J.; Lindeman, S. V.; Bennett, B.; Gardinier, J. R. *Dalton Trans.* **2011**, *40*, 8776−8787. (b) Wanniarachchi, S.; Liddle, B. J.; Toussaint, J.; Lindeman, S. V.; Bennett, B.; Gardinier, J. R. *Dalton Trans.* **2010**, *39*, 3167−3169.

(6) Wanniarachchi, S.; Liddle, B. J.; Lindeman, S. V.; Gardinier, J. R. *J. Organomet. Chem.* **2011**, *696*, 3623−3636.

(7) (a) Bursten, B. E.; Green, M. R.; Katovic, V.; Kirk, J. R.; Lightner, D., Jr. *Inorg. Chem.* **1986**, *25*, 831−834. (b) Bursten, B. E. *J. Am. Chem. Soc.* **1982**, *104*, 1299−1304.

(8) Chatt, J.; Kan, C. T.; Leigh, G. J.; Pickett, C. J.; Stanley, D. R. *J. Chem. Soc., Dalton Trans.* **1980**, 2032−2038.

(9) Lever, A. B. P. *Inorg. Chem.* **1990**, *29*, 1271−1285.

(10) Pombeiro, A. J. L. *Eur. J. Inorg. Chem.* **2007**, 1473−1482.

(11) (a) Makedonas, C.; Mitsopoulou, C. A. *Eur. J. Inorg. Chem.* **2007**, 4176−4189. (b) Ahrland, S.; Chatt, J. *J. Chem. Soc.* **1957**, 1379−1386.

(12) See Supporting Information.

(13) (a) Coe, B. J.; Fielden, J.; Foxon, S. P.; Asselberghs, I.; Clays, K.; Brunschwig, B. S. *Inorg. Chem.* **2010**, *49*, 10718−10726. (b) Shepherd, R. E.; Proctor, A.; Henderson, W. W.; Myser, T. K. *Inorg. Chem.* **1987**, *26*, 2440−2444. (c) Lavallee, D. K.; Fleischer, E. B. *J. Am. Chem. Soc.* **1972**, *94*, 2583−2599. (d) Krishna, V. G.; Chowdhury, M. *J. Phys. Chem.* **1963**, *67*, 1067−1069.

(14) Brown, S. N. *Inorg. Chem.* **2000**, *39*, 378−381.

(15) Patra, S.; Chandra, B.; Manas, K.; Maity, A. N.; Ghosh, P. *Inorg. Chem.* **2011**, *50*, 1331−1338.

(16) Kasha, M.; Rawls, R. *Photochem. Photobiol.* **1968**, *7* (6), 561−569.

(17) Selected examples: (a) Linert, W.; Kleiner, A. Thermochromism of Complexes in Solution. In *Inorganic Chromotropism: Basic Concepts and Applications of Colored Materials*; Fukuda, Y., Ed.; Springer-Verlag: New York, 2007; pp 96−99. (b) Hoggard, P. E.; Kirk, A. D. *Inorg. Chem.* **1993**, *32*, 4475−4477. (c) Suzuki, T.; Kashiwabara, K.; Kita, M.; Fujita, J.; Kaizaki, S. *Inorg. Chim. Acta* **1998**, *281*, 77−84. (d) Nagata, K.; Kanamori, K. *J. Coord. Chem.* **2002**, *55*, 925−932. (e) Ham, H. W.; Kim, Y. S. *Mol. Cryst. Liq. Cryst.* **2010**, *520*, 108−115. (f) Simonsen, K.; Hamada, M.; Suzuki, N.; Kojima, M.; Ohba, S.; Galsbøl, F.; Saito, Y.; Fujita, J. *Bull. Chem. Soc. Jpn.* **1990**, *63*, 2904−2910. (g) Jackson, W. G.; Fee, W. W. *Inorg. Chem.* **1975**, *14*, 1170−1174. (h) Kolf, S.; Preetz, W. *Z. Anorg. Allg. Chem.* **1999**, *625*, 411−416. (i) Katsuki, K.; Ooyama, Y.; Okamoto, M.; Yamamoto, Y. *Inorg. Chim. Acta* **1994**, *217* (1−2), 181−185. (j) Rosenhein, L. D.; McDonald, J. W. *J. Organomet. Chem.* **1988**, *345*, 143−149.

(18) Ballhausen, C. J. *Introduction to Ligand Field Theory*; McGraw-Hill Book Company, Inc.: New York, 1962; pp 106−108.

(19) Rathore, R.; Burns, C. L.; Deselinescu, M. I.; Denmark, S. E.; Bui, T. *Org. Synth.* **2005**, *82*, 1−9.

(20) (a) Ellison, I. J.; Gillard, R. D.; Moszner, M.; Wilgocki, M.; Ziolkowski, J. J. *J. Chem. Soc., Dalton Trans.* **1994**, 2531−2538. (b) Buckley, A. N.; Busby, J. A.; Ellison, I. J.; Gillard, R. D. *Polyhedron* **1993**, *12*, 247−253. (c) Ellison, I. J.; Gillard, R. D. *J. Chem. Soc., Chem. Commun.* **1992**, 851.

(21) Reger, D. L.; Gardinier, J. R.; Elgin, J. D.; Smith, M. D.; Hatout, D.; Long, G. J.; Grandjean, F. *Inorg. Chem.* **2006**, *45*, 8862−8875.